Achieving Multiple Functions of 3-Phase Electric Springs in Unbalanced 3-Phase Power Systems Using the Instantaneous Power Theory

Shuo Yan[1], Minghao Wang[1], Tianbo Yang[1], S. C. Tan[1], Balarko Chaudhuri[2], and S.Y.R. Hui[1,2]
[1]Department of Electrical & Electronic Engineering, The University of Hong Kong
[2]Department of Electrical & Electronic Engineering, Imperial College London

***Abstract*—Three-phase electric spring (3-ph ES) has recently been proposed as a fast demand response technology for applications in unbalanced power systems fed with a mixture of conventional and renewable power generation. Using the Instantaneous Power Theory as the theoretical framework, this paper presents the criteria and conditions for minimizing the average and oscillating power of the 3-ph ES for the first time. A detailed analysis of the use of 3-ph ES is included for providing multiple control objectives of voltage regulation and power balancing of the 3-ph power system, and minimization of the average and oscillating ac power of the ES. A corresponding control scheme implementable in a single controller is included and explained. The control scheme has been practically verified with experiments.**

Keywords— Electric spring, power balance, voltage stabilization, multifunctional control, instantaneous power theory.

I. INTRODUCTION

Power imbalance is a common and critical power quality issue in 3-ph power systems. Mild imbalance can be caused by unbalanced loading or asymmetrical grid impedance, while severe short-term imbalance can be caused by power system faults [1]. Power imbalance can result in a variety of undesirable phenomena on both power systems and equipment, such as overheating on induction motors,

large power loss, significant neutral current, poor power quality, and tripping of power converters or generators.

Solutions to tackle power imbalance have evolved from passive approaches to active approaches. Conventionally, passive filters (PFs) are used to replace bulky and expensive 3-ph to 2-ph transformers or rotating equipment. However, PFs are incapable of eliminating time-varying harmonic contents. The development of power electronic switches gives rise to active filtering techniques. Due to their fast responses, active filtering techniques (such as static var compensator (STATCOM) [1], series- and shunt-type active filters (AFs) [2], and bi-directional unified power quality conditioner (UPQC) [3]) have grown into the mainstream solutions in addressing power imbalance and harmonic issues, at the expense of high costs and complex structures. A variety of control methods have been introduced including 1) redistributing real power among three phases for power balance, 2) providing reactive power and harmonic compensation to achieve unity power factor, and 3) compensating positive-, negative-, and zero-sequence components separately or jointly.

Although these technologies can provide satisfactory compensation outcomes on various power quality issues, new methods are needed to face new challenges of emerging power grids fed by increasing penetration of renewable energy source (RES). In the regime of RES control, there is an interest in using power electronic interfaces to mitigate the adverse impact of unbalanced grid conditions. Based on instantaneous power theory [4], different control methods have been proposed to limit peak current [5], provide voltage support [6], improve current waveform [7], and remove power oscillation [8]. Although these ancillary services of RESs are valuable additions to the main function of power conversion, their availability highly depends on the disposable capacity of power converters and the accommodation of different control targets [9], [10].

Alternatively, energy storage is a useful but expensive technology [11]. Traditional demand-side management (DSM) enables “load demand following power generation [12]” but does not offer power

regulation in an instantaneous manner. With a response time in the order of milliseconds, electric spring (ES) has recently been introduced as a fast and effective DSM technology to solve various power quality issues including voltage regulation [13], [14], frequency stabilization [15], and power quality improvement [16]. 3-ph ES system and its control are reported in [17]. The combined use of energy storage, 3-ph ES, and non-critical loads allows a 3-ph ES to process a substantial amount of active power with reduced storage capacity in addition to its inherent reactive power compensation. In the original implementation in [17], the solutions of the complicated system equations are solved numerically by genetic algorithm for the ES to perform voltage regulation and current balancing. Naturally, the ES voltage references are near-optimal. Later, significant progress has been made in [18] where a theory has been developed to find the exact analytic solution of using the 3-ph ES for mitigating power imbalance in a 3-ph power supply. This theory also allows the use of the differences of the active power in the three phases to restore the power balance with minimum energy storage of the battery.

Based on the Instantaneous Power Theory [4], this project further extends the research of 3-ph ES to achieve multiple objectives of voltage regulation, reduction of power imbalance and also minimization of the oscillating active power that is not previously explored. It is found that the Instantaneous Power Theory provides a good theoretical framework for analyzing and optimizing the 3-ph power supply with ES and smart loads installed. In this paper, the performance of the 3-ph ES is improved in two critical aspects. Firstly, the multifunctional control is proposed to enable the multitasking of 3-ph ES. The key functions of voltage regulation and current balancing can be enacted simultaneously. Secondly, the active power optimization of 3-ph ES is addressed in a general case where both source voltages and currents are unbalanced. The adoption of instantaneous power theory and sequence analysis provides an accurate description of the power feature of 3-ph ES. Based on this, the proposed optimization method can not only minimize average active power but also dampen the oscillating active power. Experimental results

demonstrate that the proposed multifunctional control and active power optimization are quite effective in improving the performance of 3-ph ES.

II. Principle of the 3-phase Electric Spring

A. 3-ph Electric Spring

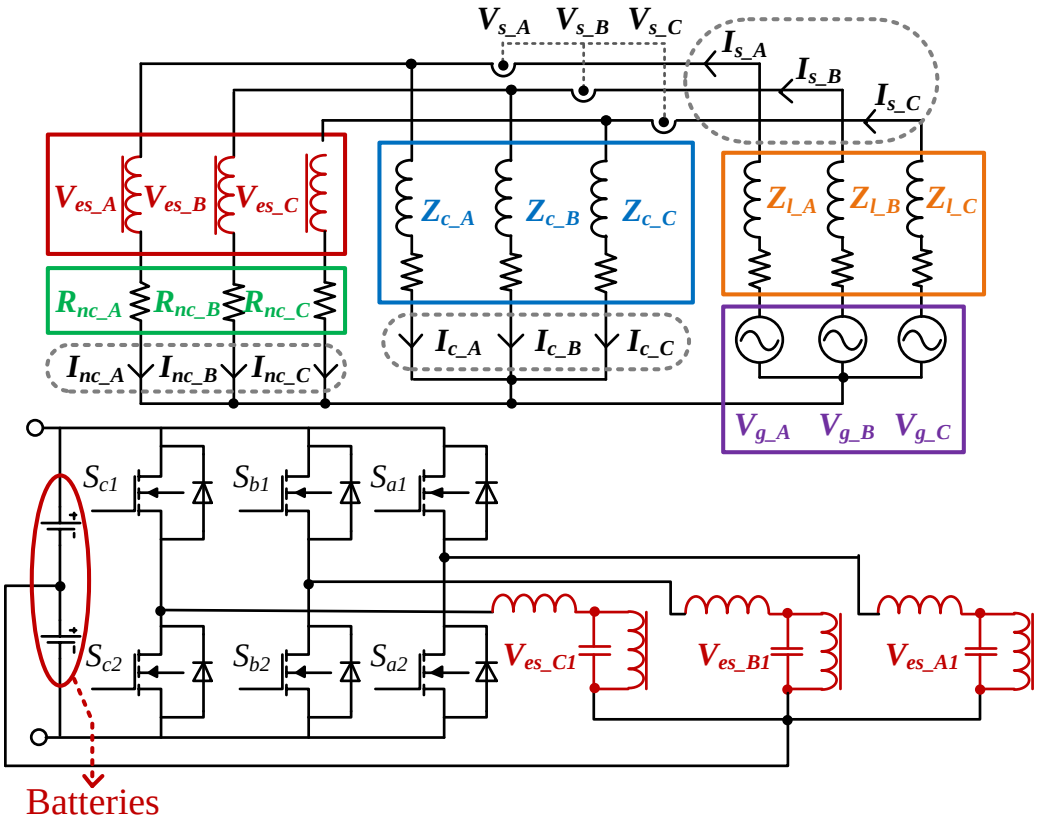

Fig. 1. The topology of a 3-ph ES [17].

Fig. 1 shows the topology of 3-ph ES. The output voltages of three inverters (i.e. V_{es_A1}, V_{es_B1}, V_{es_C1}) are filtered by *LC* filters and are coupled to the grid via isolation transformers (i.e. V_{es_A}, V_{es_B}, and V_{es_C}). The batteries on the DC link allow bidirectional active power flow. The configuration of a 3-ph inverter as an ES is unique and differs from existing power electronic facilities such as AFs, STATCOMs and series var compensators (SVCs). The series connection of ES and noncritical loads makes it possible to offer the active power consumption of noncritical loads for balancing power supply and demand, while ES also provides reactive power to regulate the mains voltage. In this way, the branch of noncritical load

and ES forms a smart load in achieving the new control paradigm of load demand following power generation. It has been demonstrated that numerous noncritical loads embedded with ES can be distributed over the grid to provide decentralized support, similar to the function of an array of mechanical springs under a mattress [19].

In this project, the multiple tasks of ac mains regulation and reduction of the power imbalance are the objectives. In Fig. 1, the loads are divided into the critical loads and the noncritical loads. Through the 3ph transformer, the 3-phase inverter provides three phase voltages (V_{es_A}, V_{es_B}, and V_{es_C}) that may or may not be identical in terms of root-mean-square values. The compensation voltage for each phase (V_{es_A}, V_{es_B}, and V_{es_C}) is inserted into the main power system so that the phase voltage of the ac mains (V_{s_A}, V_{s_B}, and V_{s_C}) is equal to the vectorial sum of the ES coupled voltage (V_{es_A}, V_{es_B}, and V_{es_C}) and the corresponding noncritical load voltage (V_{nc_A}, V_{nc_B} and V_{nc_C}).

A uniqueness of the ES operation is to utilize input voltage control so that the input voltages (i.e. phase voltages of the ac mains) are regulated by the ES, whilst the outputs of ES are allowed to fluctuate in order to provide three adaptive voltages across the noncritical loads (V_{nc_A}, V_{nc_B} and V_{nc_C}). These three voltages can be considered as an adaptive 3-ph voltage source for the noncritical load. Therefore, the operation of the ES leads to a standard ac mains (that is well regulated) and an adaptive ac mains (that has a relatively larger fluctuating voltage range). The purpose of this dual ac mains arrangement is to use the noncritical load to absorb as much as possible the fluctuating power from the power source caused by the intermittent renewable power generation.

Regarding the objective of reducing power imbalance, it should be noted that the critical loads in the three-phase power system of a typical building are usually not balanced. Any power imbalance in the three-phase power system of a building will cause a non-zero neutral current, which in turn gives rise to unwanted conduction power losses. Since the three inverter-legs share the same dc voltage link, the

inverter of the ES can be controlled in order to use the noncritical loads to reduce the power imbalance in the critical loads.

B. Multifunctional Operation

Based on the circuit diagram given in Fig. 1, the vector equation of the noncritical load current is given in (1). For simplicity of analysis, the noncritical load is assumed to be resistive, although it is not a necessary condition [14], [20], and [21]. For simultaneous voltage and current compensations, the ES voltages are further decomposed into $V_{es\_A/B/C\_v}$ and $V_{es\_A/B/C\_i}$. One can further derive (3) by reorganizing (2). In (3), the first part of the ES voltage ($V_{es\_A/B/C\_v}$) is used to stabilize the mains voltage. This part of the ES voltage in each phase varies in the same fashion to change the noncritical load current so that the mains voltage can be supported and suppressed. The second part of the ES voltage ($V_{es\_A/B/C\_i}$) changes individually in compensating the unbalanced currents of the critical load.

$$\begin{cases} I_{nc\_A} = \dfrac{V_{s\_A} - V_{es\_A}}{R_{nc\_A}} \\ I_{nc\_B} = \dfrac{V_{s\_B} - V_{es\_B}}{R_{nc\_B}} \\ I_{nc\_C} = \dfrac{V_{s\_C} - V_{es\_C}}{R_{nc\_C}} \end{cases} \tag{1}$$

$$\begin{cases} I_{nc\_A} = \dfrac{V_{s\_A} - (V_{es\_A\_v} + V_{es\_A\_i})}{R_{ncA}} \\ I_{nc\_B} = \dfrac{V_{s\_B} - (V_{es\_B\_v} + V_{es\_B\_i})}{R_{nc\_B}} \\ I_{nc\_C} = \dfrac{V_{s\_C} - (V_{es\_C\_v} + V_{es\_C\_i})}{R_{nc\_C}} \end{cases} \tag{2}$$

$$\begin{cases} I_{nc\_A} = \dfrac{V_{s\_A} - V_{es\_A\_v}}{R_{ncA}} - \dfrac{V_{es\_A\_i}}{R_{ncA}} \\ I_{nc\_B} = \dfrac{V_{s\_B} - V_{es\_B\_v}}{R_{nc\_B}} - \dfrac{V_{es\_B\_i}}{R_{nc\_B}} \\ I_{nc\_C} = \dfrac{V_{s\_C} - V_{es\_C\_v}}{R_{nc\_C}} - \dfrac{V_{es\_C\_i}}{R_{nc\_C}} \end{cases} \tag{3}$$

The idea of controlling the 3-ph ES to conduct both voltage regulation and power balancing can be summarized as:

- $V_{es\_A/B/C\_i}$ in each phase provides independent compensation to balance the active and reactive current of the critical load.

- After the 3-ph critical load is balanced, $V_{es\_A/B/C\_v}$ boosts or reduces the power consumption of the noncritical load to match the fluctuating power of RESs. Therefore, the mains voltage can be stabilized at its nominal value.

A set of vector illustrations is shown in Fig. 2 to give a detailed explanation of the principle. Three states of the system are included in the vector illustrations, namely uncompensated state in Fig. 2(a), current balancing state in Fig. 2(b), and current balancing plus voltage stabilization state in Fig. 2(c). In the uncompensated system, the source current is unbalanced due to the existence of asymmetric critical load. In Fig. 2(a), the green vectors, the purple vectors, and the red vectors are respectively the critical load currents ($I_{c\_A/B/C}$), the noncritical load currents ($I'_{nc\_A/B/C}$), and the source currents ($I_{s\_A/B/C}$) in the uncompensated state. The 3-ph ES is firstly activated to introduce the compensation currents $\Delta I_{nc\_A/B/C\_i} = \dfrac{V_{es\_A/B/C\_i}}{R_{nc\_A/B/C}}$ (the blue dotted vectors) for current balancing, which is added up to the uncompensated $I'_{nc\_A/B/C}$. The noncritical load current is changed to $I_{nc\_A/B/C}$ (blue solid vector). Therefore, $I_{s\_A/B/C}$ are compensated into the symmetrical state as in Fig. 2(b). After the 3-ph system is compensated to be symmetrical, the second part of compensation currents is introduced by the 3-ph ES to further modulate the 3-ph source currents. As indicated in the vector diagram in Fig. 2(c),

$\Delta I_{nc\_A/B/C\_v} = \frac{V_{es\_A/B/C\_v}}{R_{nc\_A/B/C}}$ (the brown dotted vectors) are used to reduce the 3-ph source currents for an equal amount. The 3-ph mains voltages can thus be supported whilst the 3-ph source currents are maintained to be balanced. The red vectors in Fig. 2(c) show that the 3-ph source currents is symmetric and reduced for simultaneous current balancing and voltage support. The reverse operation of using $\Delta I_{nc\_A/B/C\_v}$ to suppress the 3-ph mains voltages is possible as well.

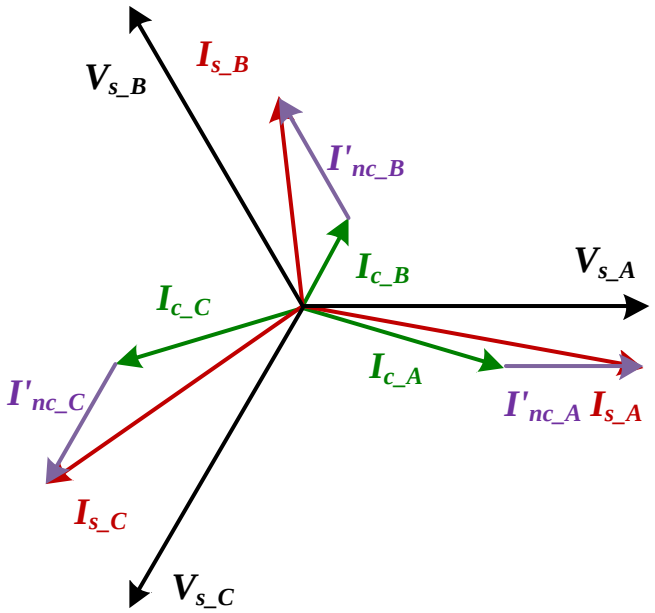

(a)

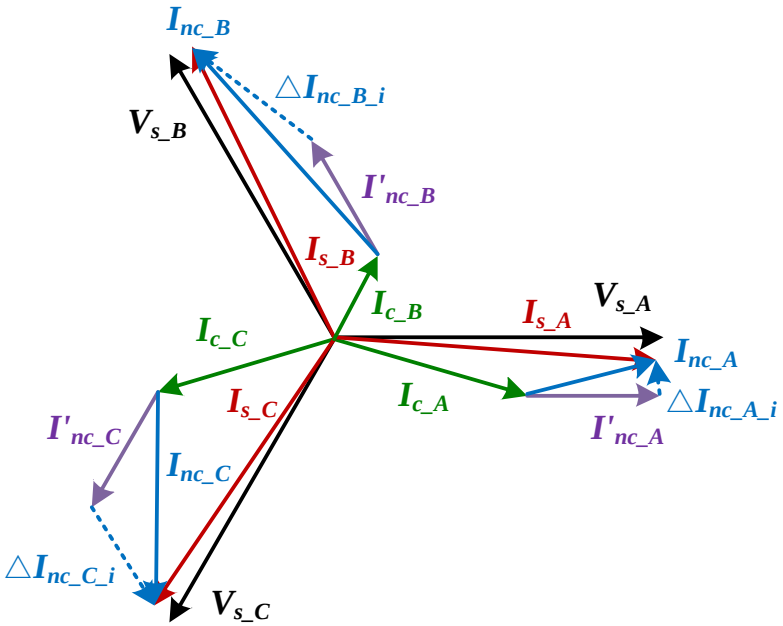

(b)

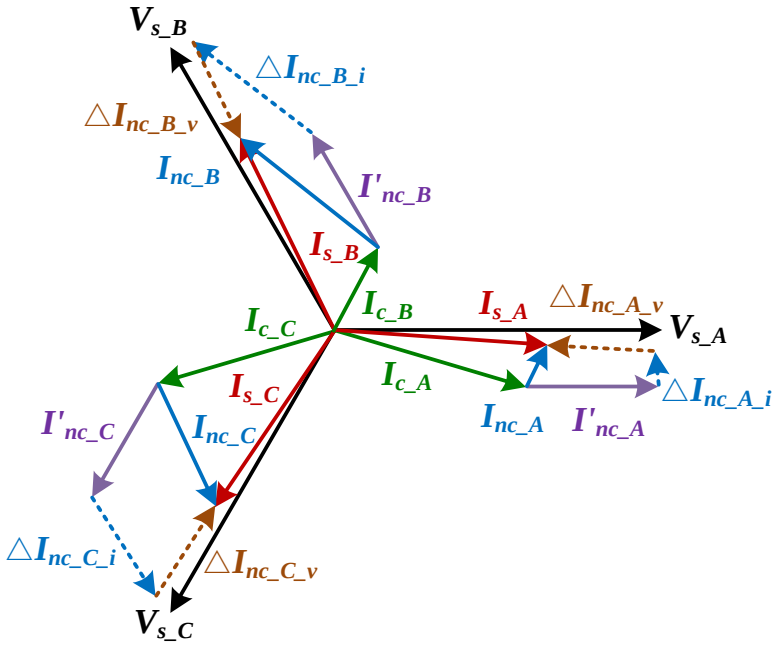

(c)

Fig. 2. Vector illustrations of a decoupled 3-ph system compensated by 3-ph ES. (a) Uncompensated states. (b) Current balancing. (c) Current balancing plus voltage regulation.

It can be seen from Fig. 2 that the capability of the 3-ph ES in current balancing and voltage regulation depends on the variable range of noncritical load current (i.e. $\Delta I_{nc\_A/B/C} = \Delta I_{nc\_A/B/C\_i} + \Delta I_{nc\_A/B/C\_v}$). This load-dependent characteristic was studied in [21]. Two general conclusions are drawn as 1) the power factor of the noncritical load does not affect $\Delta I_{nc\_A/B/C}$, while the voltage rating of the ES and the impedance of noncritical load determine the size of the dispatchable range, and 2) the power factor of the noncritical load has an impact on the power decoupling of the ES. Hence, there is a preference of using noncritical load having near-unity power factor for the simplification of control structure and mathematical analysis.

III. Instantaneous Power Optimization

A. Circuit Analysis

The source current references can be set arbitrarily to derive a balanced 3-ph source current. Hence, it is necessary to determine one optimal set of references that achieves the minimal active power

usage of 3-ph ES. It should be highlighted that the optimization problem in this paper is addressed in a general case where the source voltage and source current are both unbalanced. The adoption of instantaneous power theory allows the active power of 3-ph ES to be more delicately handled with the consideration of both average and oscillating components.

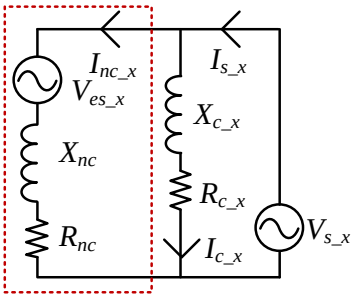

Fig. 3. Per-phase model of a 3-ph system. (Note: *x* refers to phase A, B, or C in the 3-ph system.)

Fig. 3 shows the per-phase model of the 3-ph system shown in Fig. 1. It consists of a source voltage (V_{s_x}), a critical load ($R_{c\_x}+jX_{c\_x}$), an ES modeled as a controllable voltage source (V_{es_x}), and a resistive noncritical load (R_{nc}). The 3-ph noncritical load (R_{nc}) is assumed to be balanced, so the notation "*x*" is not used. The noncritical load current can be derived as

$$I_{nc\_x} = \frac{V_{s\_x} - V_{es\_x}}{R_{nc}} \tag{4}$$

According to Kirchhoff's current law, it is easy to derive

$$I_{s\_x} = I_{c\_x} + I_{nc\_x} \tag{5}$$

Eq. (5) is illustrated by the vector diagram in Fig. 4. It shows that by adding the noncritical load current controlled by the ES (the blue vector, I_{nc_x}) to the critical load current (green vector, I_{c_x}), the source current can be compensated to the expected value (the red vector, I_{s_x}).

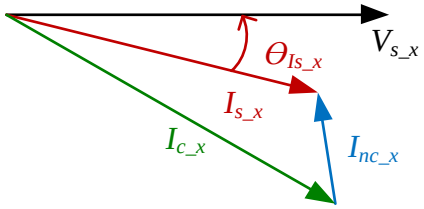

Fig. 4. The vector diagram of the circuit in Fig. 3. (Note: *x* refers to phase A, B, or C in the 3-ph system)

Inserting (4) into (5), one can derive (6) after some mathematical manipulations.

$$V_{es\_x} = V_{s\_x} - R_{nc}\left(I_{s\_x} - I_{L\_x}\right) \tag{6}$$

Eqn. (6) indicates that the ES voltage reference $V^{*}_{es\_x}$ can be derived by setting I_{s_x} to its reference value $I^{*}_{s\_x}$.

B. The Optimization of Instantaneous Active Power

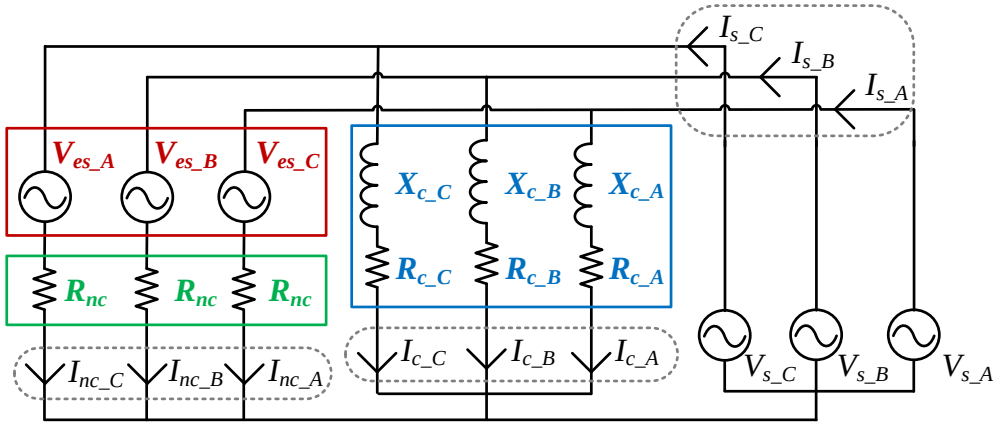

Fig. 5. The 3-ph circuit model.

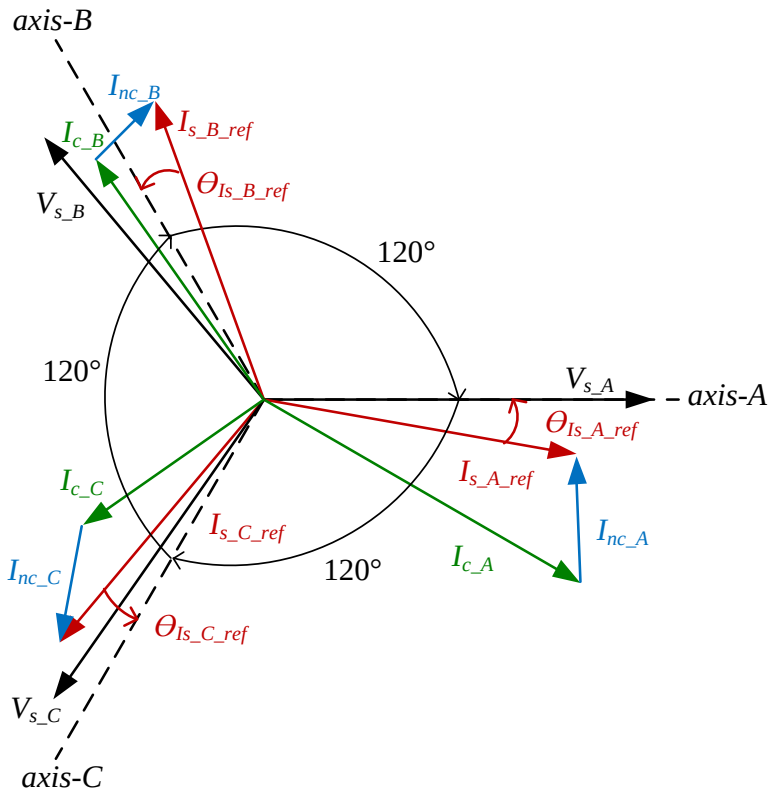

Fig. 6. The vector diagram of Fig. 5.

The per-phase model derived in Fig. 3 is expanded to a general unbalanced 3-ph system as given in Fig. 5. The corresponding vector diagram is shown in Fig. 6. In Fig. 6, the mains voltage of phase-A is selected as the reference axis (denoted as *axis-A*) with 0° phase angle. By rotating *axis-A* for 240° and 120° clockwise, the reference axis for phase-B and phase-C are derived, which are denoted as *axis-B* and *axis-C* respectively. *Axis-A*, *axis-B*, and *axis-C* form a 3-ph stationary reference frame, where the phase angle of other voltage and current vectors can be determined. (7) and (8) can be used to describe the operating state of the circuit in Fig. 5.

$$\begin{pmatrix} V^*_{es\_A} \\ V^*_{es\_B} \\ V^*_{es\_C} \end{pmatrix} = \begin{pmatrix} V_{s\_A} \\ V_{s\_B} \\ V_{s\_C} \end{pmatrix} - R_{nc} \left(\begin{pmatrix} I^*_{s\_A} \\ I^*_{s\_B} \\ I^*_{s\_C} \end{pmatrix} - \begin{pmatrix} I_{c\_A} \\ I_{c\_B} \\ I_{c\_C} \end{pmatrix} \right) \tag{7}$$

$$\begin{pmatrix} I_{nc\_A} \\ I_{nc\_B} \\ I_{nc\_C} \end{pmatrix} = \frac{1}{R_{nc}} \left(\begin{pmatrix} V_{s\_A} \\ V_{s\_B} \\ V_{s\_C} \end{pmatrix} - \begin{pmatrix} V^*_{es\_A} \\ V^*_{es\_B} \\ V^*_{es\_C} \end{pmatrix} \right) \tag{8}$$

For a perfect compensation, the 3-ph source current reference ($I^*_{s\_A/B/C}$) should be well balanced and does not contain any negative- and zero-sequence components. Applying Clark transformation and introducing positive-, negative-, and zero-sequence components on ES voltage and noncritical load current, one can derive

$$\mathbf{V}^*_{es} = \begin{pmatrix} \mathbf{V}^*_{es\_\alpha} \\ \mathbf{V}^*_{es\_\beta} \\ \mathbf{V}^*_{es\_0} \end{pmatrix} = \begin{pmatrix} \mathbf{V}^{*+}_{es\_\alpha} + \mathbf{V}^{*-}_{es\_\alpha} \\ \mathbf{V}^{*+}_{es\_\beta} + \mathbf{V}^{*-}_{es\_\beta} \\ \mathbf{V}^*_{es\_0} \end{pmatrix} = \begin{pmatrix} V^+_{es}\sin(\omega t + \theta_{Ves+}) + V^-_{es}\sin(\omega t + \theta_{Ves-}) \\ -V^+_{es}\cos(\omega t + \theta_{Ves+}) + V^-_{es}\cos(\omega t + \theta_{Ves-}) \\ V^0_{es}\sin(\omega t + \theta_{Ves0}) \end{pmatrix} \tag{9}$$

$$\mathbf{I}_{nc} = \begin{pmatrix} \mathbf{I}_{nc\_\alpha} \\ \mathbf{I}_{nc\_\beta} \\ \mathbf{I}_{nc\_0} \end{pmatrix} = \begin{pmatrix} \mathbf{I}^+_{nc\_\alpha} + \mathbf{I}^-_{nc\_\alpha} \\ \mathbf{I}^+_{nc\_\beta} + \mathbf{I}^-_{nc\_\beta} \\ \mathbf{I}_{nc\_0} \end{pmatrix} = \begin{pmatrix} I^+_{nc}\sin(\omega t + \theta_{Inc+}) + I^-_{nc}\sin(\omega t + \theta_{Inc-}) \\ -I^+_{nc}\cos(\omega t + \theta_{Inc+}) + I^-_{nc\_\beta}\cos(\omega t + \theta_{Inc-}) \\ I^0_{nc}\sin(\omega t + \theta_{Inc0}) \end{pmatrix} \tag{10}$$

According to instantaneous power theory [4], the active power of the ES can be derived as

$$\begin{aligned} p_{es} &= \mathbf{V}^*_{es\_\alpha} \cdot \mathbf{I}_{nc\_\alpha} + \mathbf{V}^*_{es\_\beta} \cdot \mathbf{I}_{nc\_\beta} + \mathbf{V}^*_{es\_0} \cdot \mathbf{I}_{nc\_0} \\ &= \overline{P_{es}} + P_{es\_c2} \cdot \cos(2\omega t) + P_{es\_s2} \cdot \sin(2\omega t) \end{aligned} \tag{11}$$

, where $\overline{P_{es}}$ is the average part of the active power, P_{es_c2} and P_{es_s2} are amplitudes of the oscillating active power at twice the system frequency, which can be computed as

$$\begin{pmatrix} \overline{P_{es}} \\ P_{es\_c2} \\ P_{es\_s2} \end{pmatrix} = \frac{3}{2} \begin{pmatrix} V^{*+}_{es\_d} & V^{*+}_{es\_q} & V^{*-}_{es\_d} & V^{*-}_{es\_q} & V^{*0}_{es\_\mathrm{Re}} & V^{*0}_{es\_\mathrm{Im}} \\ V^{*-}_{es\_d} & V^{*-}_{es\_q} & V^{*+}_{es\_d} & V^{*+}_{es\_q} & V^{*0}_{es\_\mathrm{Re}} & -V^{*0}_{es\_\mathrm{Im}} \\ V^{*-}_{es\_q} & -V^{*-}_{es\_d} & -V^{*+}_{es\_q} & V^{*+}_{es\_d} & -V^{*0}_{es\_\mathrm{Im}} & -V^{*0}_{es\_\mathrm{Re}} \end{pmatrix} \begin{pmatrix} I^+_{nc\_d} \\ I^+_{nc\_q} \\ I^-_{nc\_d} \\ I^-_{nc\_q} \\ I^0_{nc\_\mathrm{Re}} \\ I^0_{nc\_\mathrm{Im}} \end{pmatrix} \tag{12}$$

In (12), a positive *d-q* synchronous reference frame, a negative *d-q* synchronous reference frame, and a zero *Re-Im* synchronous reference frame are applied, respectively, to the positive-, negative-, and

zero-sequence voltages/currents. Each of the components in the corresponding positive-, negative-, and zero-frame in (12) can be written as

$$V_{es\_d}^{*+} = V_{s\_d}^{+} - R_{nc}\left(I_{s\_d}^{*} - I_{c\_d}^{+}\right) \tag{13}$$

$$V_{es\_q}^{*+} = V_{s\_q}^{+} - R_{nc}\left(I_{s\_q}^{*} - I_{c\_q}^{+}\right) \tag{14}$$

$$V_{es\_d}^{*-} = V_{s\_d}^{-} - R_{nc}\left(-I_{c\_d}^{-}\right) \tag{15}$$

$$V_{es\_q}^{*-} = V_{s\_q}^{-} - R_{nc}\left(-I_{c\_q}^{-}\right) \tag{16}$$

$$I_{nc\_d}^{+} = \frac{1}{R_{nc}}\left(V_{s\_d}^{+} - V_{es\_d}^{*+}\right) \tag{17}$$

$$I_{nc\_q}^{+} = \frac{1}{R_{nc}}\left(V_{s\_q}^{+} - V_{es\_q}^{*+}\right) \tag{18}$$

$$I_{nc\_d}^{-} = \frac{1}{R_{nc}}\left(V_{s\_d}^{-} - V_{es\_d}^{*-}\right) \tag{19}$$

$$I_{nc\_q}^{-} = \frac{1}{R_{nc}}\left(V_{s\_q}^{-} - V_{es\_q}^{*-}\right) \tag{20}$$

$$V_{es\_\mathrm{Re}}^{*0} = V_{s\_\mathrm{Re}}^{0} - R_{nc}\left(-I_{c\_\mathrm{Re}}^{0}\right) \tag{21}$$

$$V_{es\_\mathrm{Im}}^{*0} = V_{s\_\mathrm{Im}}^{0} - R_{nc}\left(-I_{c\_\mathrm{Im}}^{0}\right) \tag{22}$$

$$I_{nc\_\mathrm{Re}}^{0} = \frac{1}{R_{nc}}\left(V_{s\_\mathrm{Re}}^{0} - V_{es\_\mathrm{Re}}^{*0}\right) \tag{23}$$

$$I_{nc\_\mathrm{Im}}^{0} = \frac{1}{R_{nc}}\left(V_{s\_\mathrm{Im}}^{0} - V_{es\_\mathrm{Im}}^{*0}\right) \tag{24}$$

Inserting (13) to (24) into (12), the full expansion of $\overline{P_{es}}$ are given in (25). It is easy to observe that $\overline{P_{es}}$ can be controlled by manipulating the source current references ($I_{s\_d}^{*}$ and $I_{s\_q}^{*}$). One can further observe that the change of source current references only changes the part of $\overline{P_{es}}$ containing positive-

sequence components ($\overline{P_{es}^{+}}$) but not the other two with negative-sequence components ($\overline{P_{es}^{-}}$) and zero-sequence component ($\overline{P_{es}^{0}}$). Hence, it is possible to use $\overline{P_{es}^{+}}$ to compensate $\overline{P_{es}^{-}} + \overline{P_{es}^{0}}$ so that $\overline{P_{es}}$ can become zero.

$$\begin{aligned}\overline{P_{es}} &= \overline{P_{es}^{+}} + \overline{P_{es}^{-}} + \overline{P_{es}^{0}} \\ &= \frac{3}{2}\left[V_{s\_d}^{+}\left(I_{s\_d}^{*} - I_{c\_d}^{+}\right) - R_{nc}\left(I_{s\_d}^{*} - I_{c\_d}^{+}\right)^2 + V_{s\_q}^{+}\left(I_{s\_q}^{*} - I_{c\_q}^{+}\right) - R_{nc}\left(I_{s\_q}^{*} - I_{c\_q}^{+}\right)^2\right] \\ &\quad -\frac{3}{2}\left[I_{c\_d}^{-}V_{s\_d}^{-} + R_{nc}\left(I_{c\_d}^{-}\right)^2 + I_{L\_q}^{-}V_{s\_q}^{-} + R_{nc}\left(I_{c\_q}^{-}\right)^2\right] \\ &\quad -\frac{3}{2}\left[I_{c\_\mathrm{Re}}^{0}\cdot V_{s\_\mathrm{Re}}^{0} + R_{nc}\cdot\left(I_{c\_\mathrm{Re}}^{0}\right)^2 + I_{c\_\mathrm{Im}}^{0}\cdot V_{s\_\mathrm{Im}}^{0} + R_{nc}\cdot\left(I_{c\_\mathrm{Im}}^{0}\right)^2\right]\end{aligned} \tag{25}$$

After some mathematic manipulations, (25) can be further written as (26).

$$\overline{P_{es}} = \frac{3}{2}R_{nc}\left[\left(x-a\right)^2 + \left(y-b\right)^2 - c\right] \tag{26}$$

, where $x = I_{s\_d}^{*} - I_{c\_d}^{+}$, $y = I_{s\_q}^{*} - I_{c\_q}^{+}$, $a = \frac{V_{s\_d}^{+}}{2R_{nc}}$, $b = \frac{V_{s\_q}^{+}}{2R_{nc}}$, $c = \frac{\left(V_{s\_d}^{+}\right)^2 + \left(V_{s\_q}^{+}\right)^2}{4R_{nc}^2} + \frac{2\left(\overline{P_{es}^{-}} + \overline{P_{es}^{0}}\right)}{3R_{nc}}$.

TABLE I. COMPENSATION STATES

Value of c	**Minimization of $\overline{P_{es}}$**	**Minimization of $\left\|\overline{P_{es}}\right\|$**
$c > 0$	✓	✓
$c = 0$	✓	×
$c < 0$	✓	×

This average power equation (26) in the d-q frame is similar to the circular paraboloid function for the abc frame first mentioned in [18]. Three optimization states of $\overline{P_{es}}$, $\overline{P_{es\_c2}}$ and $\overline{P_{es\_s2}}$ are possible with different values of *c*, which are summarized in TABLE I. With the two values of *c* ($c < 0$ and $c = 0$), the optimization can only be done towards the minimization of $\overline{P_{es}}$. However, if $c > 0$, a circle can be defined by (26) on a 2-D plenary by setting $\overline{P_{es}} = 0$. In this case, there are infinite pairs of *x* and *y* that

lead to a zero $\overline{P_{es}}$. It is further possible to use one of them to minimize the oscillating power of 3-ph ES ($\tilde{P}_{es\_c2}$ and $\tilde{P}_{es\_s2}$).

The advantage of using the Instantaneous Power Theory as the theoretical framework is that it provides the oscillating active power components that are not available in the traditional steady-state analysis of power systems. The objective function can be set as

$$Obj = \left(\tilde{P}_{es}\right)^2 = \left(\tilde{P}_{es\_c2}\right)^2 + \left(\tilde{P}_{es\_s2}\right)^2 = (Ax + By + C)^2 + (Dx + Ey + F)^2 \tag{27}$$

, where

$$A = 2R_{nc} \cdot I^{-}_{c\_d} + V^{-}_{s\_d}$$

$$B = 2R_{nc} \cdot I^{-}_{c\_q} + V^{-}_{s\_q}$$

$$C = -I^{-}_{c\_d} \cdot V^{+}_{s\_d} - I^{-}_{c\_q} \cdot V^{+}_{s\_q} + \tilde{P}^{0}_{es\_c2}$$

$$D = B,\ E = -A$$

$$F = I^{-}_{c\_d} \cdot V^{+}_{s\_q} - I^{-}_{c\_q} \cdot V^{+}_{s\_d} + \tilde{P}^{0}_{es\_s2}$$

$$\tilde{P}^{0}_{es\_c2} = -I^{0}_{c\_\mathrm{Re}} \cdot V^{0}_{s\_\mathrm{Re}} - R_{nc} \cdot \left(I^{0}_{L\_\mathrm{Re}}\right)^2 + I^{0}_{c\_\mathrm{Im}} \cdot V^{0}_{s\_\mathrm{Im}} + R_{nc} \cdot \left(I^{0}_{c\_\mathrm{Im}}\right)^2$$

$$\tilde{P}^{0}_{es\_s2} = I^{0}_{c\_\mathrm{Im}} \cdot V^{0}_{s\_\mathrm{Re}} + I^{0}_{c\_\mathrm{Re}} \cdot V^{0}_{s\_\mathrm{Im}} + 2R_{nc} I^{0}_{c\_\mathrm{Re}} \cdot I^{0}_{c\_\mathrm{Im}}$$

Rewriting x and y as trigonometric functions in (28) and (29), the objective function can be transformed into a single variable function in respect to θ.

$$x = a + \sqrt{c}\cos\theta \tag{28}$$

$$y = b + \sqrt{c}\sin\theta \tag{29}$$

The value of θ is determined to derive the minimum value of $\left(\tilde{P}_{es}\right)^2$. The corresponding pair of x and y is the optimized solution of zero $\overline{P_{es}}$ and minimum $\tilde{P}_{es}$. To avoid solving complex trigonometric equations,

a simple online searching approach is adopted to find the minimum value of (27), which can be easily implemented in the digital controller. The flow chart of searching the minimum value of (27) is given in Fig. 7. The value of θ starts at 2° and increases 2° at each step until 360°. The value of θ is inserted into (27)-(29) to calculate the value of the objective function at each step. The value of the objective function at the n^{th} step is compared with the result acquired at the $(n-1)^{th}$ step. The smaller value and the corresponding θ are kept for the comparison at the $(n+1)^{th}$ step. At the end of the searching process (i.e. $n = 180$), the θ with the minimum value of *Obj* in (27) is used for converter control.

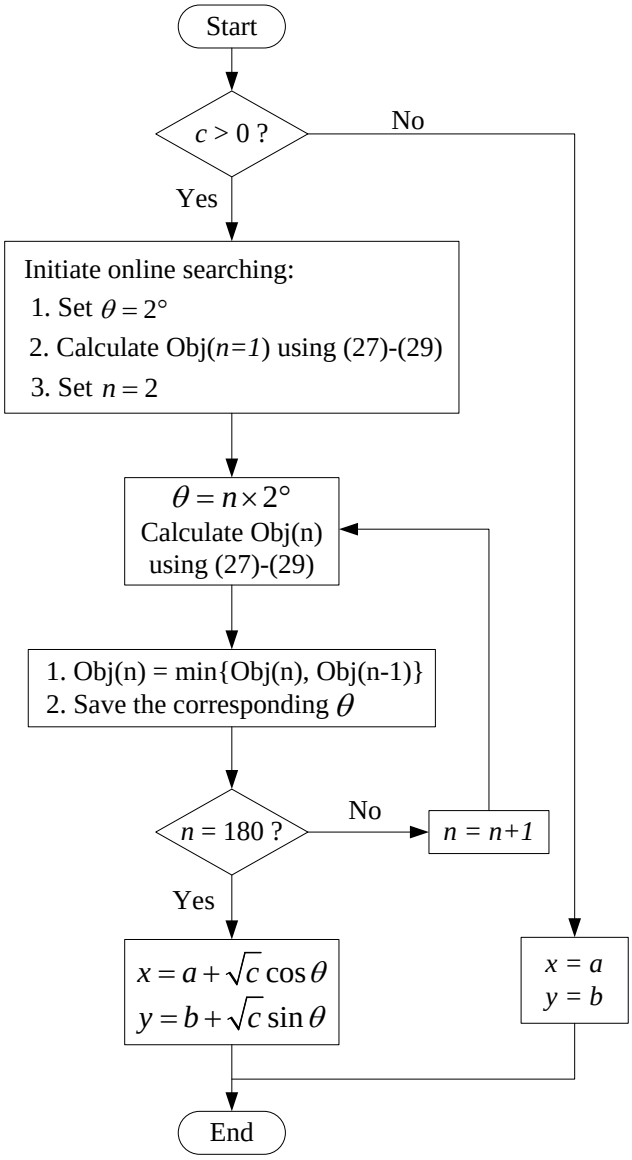

Fig. 7. Flow chart of online search for the minimum value of the objective function (27).

C. Numerical Example

TABLE II. SPECIFICATIONS OF THE NUMERICAL EXAMPLE

Specifications of Implementation			
	Phase A	Phase B	Phase C
$\vec{Z}_c$ (Ω) Critical	500 (resistive)	250 – *j* 116 (resistive -inductive)	115 + *j* 127 (resistive- capacitive)
R_{nc} (Ω) Noncritical	200 (resistive)	200 (resistive)	200 (resistive)
Source Voltages (RMS)	220∠0°	230∠240°	215∠120°
Steady-State Operating Parameters			
	Positive-Sequence	Negative-Sequence	Zero-Sequence
$\boldsymbol{V_s}$	313. 4∠0° = 313.4 + 0j	6.2∠101° = –1.18 + 6.09j	6.2∠–101° = –1.18 – 6.09j
$\boldsymbol{I_c}$	1∠16° = 0.96 + 0.28j	0.39∠–26° = 0.35 – 0.17j	0.70∠–172° = –0.69 – 0.10j
ES Compensation Voltages			
	$\mathbf{V_{es\_A}}$	$\mathbf{V_{es\_B}}$	$\mathbf{V_{es\_C}}$
Optimized	×	×	×
Near-Optimized	102.3∠327°	246.1∠201°	282.8∠167°
Un-optimized	55.6∠351°	193.4∠206°	300.2∠178°

One numerical example is provided here to demonstrate the proposed optimization approach. The circuit follows the one in Fig. 1 with the specifications tabulated in TABLE II. The steady-state positive-, negative-, and zero-sequence components of currents and voltages are also included in TABLE II. Inserting them into (26), $\overline{P_{es}}$ can be derived as

$$\overline{P_{es}} = \left(x - 0.784\right)^2 + y^2 + 0.028 \tag{30}$$

Since c = -0.028 in (30) is negative, the 3-ph system can only be optimized to have the minimum average active power. The corresponding ES compensation voltages are given in TABLE II in the row of "Near-Optimized", while the row of "Optimized" is inapplicable for this numerical example.

For the purpose of comparison, one more group of simulation results acquired from another set of ES voltages is included. In TABLE II, the set of ES voltages in row termed as "Un-optimized" can only balance the source current but not achieve minimized $\overline{P_{es}}$ and P_{es}. The simulation results of the ES power and the source current are included in Fig. 8 and Fig. 9. It can be observed that the $\overline{P_{es}}$ and P_{es} acquired by

using the “Near-optimized” ES voltages is smaller than those acquired from “Un-optimized” ES voltages (Fig. 8) when both of them shows an equal ability to balance the source current (Fig. 9).

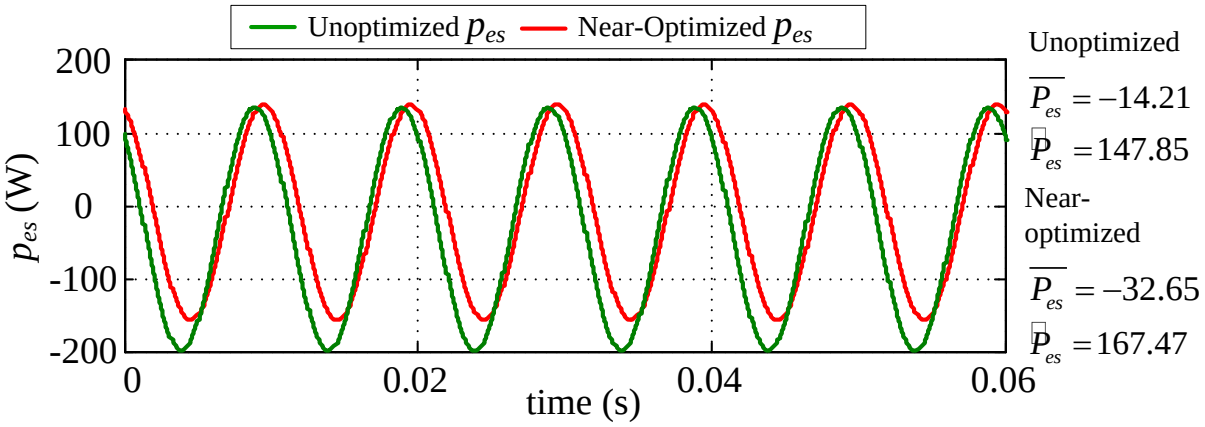

Fig. 8. The instantaneous active power of 3-ph ES. (Note: $\overline{P_{es}}$ and $\hat{P}_{es}$ are respectively the DC offset and the amplitude of sinusoidal waveforms.)

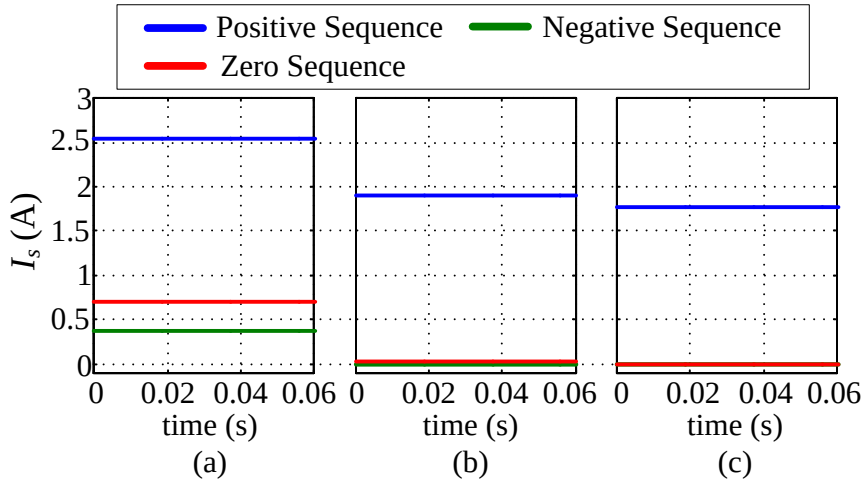

Fig. 9. Positive-, negative-, and zero-sequences of source currents. (a) Un-compensated. (b) Un-optimized. (c) Near-Optimized.

IV. Control Structure

In this section, the structure of the multifunctional control is discussed. Fig. 10 shows the block diagram of the proposed control loops. The control system consists of two parts. One part is implemented for voltage regulation, and the other is operated for source current balancing and instantaneous active power optimization. The aspects of control targets can be summarized as: 1) current balancing and

instantaneous active power optimization highlighted in the red dotted block, 2) voltage regulation highlighted in the blue dotted block, and 3) the simultaneous operation of the above two functions.

The part of the controller highlighted in the blue dotted rectangle shows the control loops for voltage regulation. The positive-sequence of the mains voltage is fed back and compared with its nominal reference value (e.g. 220 V). Two Proportional-Integral (PI) controllers are implemented to regulate the real ($V^{+}_{es\_v\_d}$) and imagine ($V^{+}_{es\_v\_q}$) components of the ES voltage references in positive-sequence. (31) and (32) give the mathematic expressions of these two controllers. The derived references ($V^{+}_{es\_v\_d}$ and $V^{+}_{es\_v\_q}$) are used to regulate the positive-sequence active and reactive power of the noncritical load. This part of ES voltage reference is denoted as $V^{+}_{es\_A/B/C\_v}$. It is a fully balanced value, which can change the power of the 3-ph noncritical load in a symmetric fashion.

$$V^{+}_{es\_v\_d} = \left(V^{+}_{s\_rms\_ref} - V^{+}_{s}\right)\left(K_{P\_q} + K_{I\_q}\frac{1}{s}\right) \tag{31}$$

$$V^{+}_{es\_v\_q} = \left(V^{+}_{s\_rms\_ref} - V^{+}_{s}\right)\left(K_{P\_q} + K_{I\_q}\frac{1}{s}\right) \tag{32}$$

The second part of the controller highlighted in the red dotted box shows the current balancing loops with active power optimization. Two sequence-extractors are used to acquire the positive-, negative-, and zero-sequence components of critical load currents and source voltages. (25) to (29) derived in Section III are used to determine the optimization state and calculate the corresponding source current references. The source current reference ($I^{*}_{s\_A/B/C}$) is perfectly balanced and consists of only positive-sequence value. The ES voltage references for current balancing ($V^{*}_{es\_A/B/C\_i}$) are derived by applying (7).

The ES voltage references ($V^{*}_{es\_A/B/C}$) are the sum of the first parts for voltage stabilization ($V^{*+}_{es\_A/B/C\_v}$) and the second parts for current balancing ($V^{*}_{es\_A/B/C\_i}$).The derived ES voltage references

will be sent to the inverter controllers in the next stage. The synchronization of the ES voltage is achieved via the popular phase lock loop (PLL) technology proposed in [22], while the improved PLL technology is a possible replacement to improve the precision and speed of synchronization under unbalanced grid conditions [23].

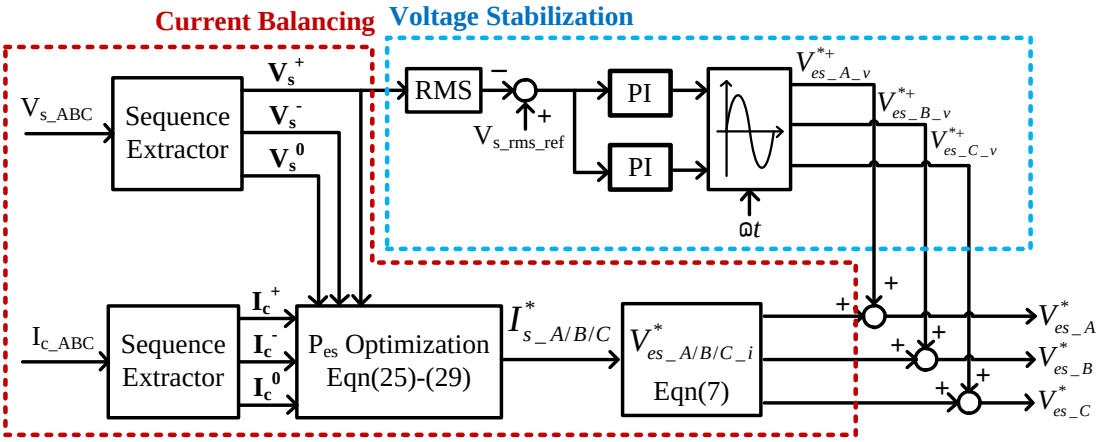

Fig. 10. The proposed multifunctional control of 3-ph ES.

V. Experimental Results

A. *Tests on the Multifunctional Control*

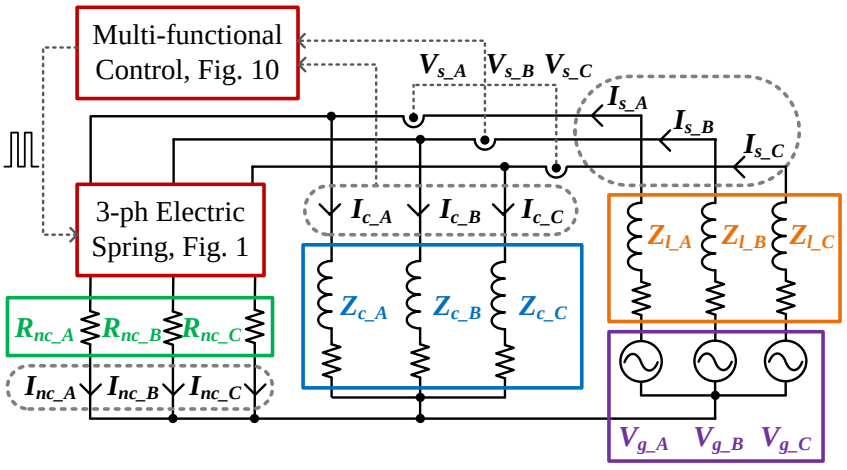

Fig. 11. The schematic of the experimental setup.

In this section, the effectiveness of the multifunctional control is practically evaluated. Fig. 11 shows the schematic of the experimental setup, in which a power source, a distribution line emulator, a 3-

ph ES, a 3-ph noncritical load, and two 3-ph critical loads are included. TABLE III gives the specifications of the hardware setup. Two sets of experiments have been conducted to test the operation of the 3-ph ES for providing both voltage stabilization and power balancing. In the first experiment, the 3-ph ES is programmed to balance the source current and support the mains voltage. The two main control objectives are tested individually and then collectively. The second experiment repeats the function of the 3-ph ES to balance the source current and tests its ability to suppress the main voltage. The individual and collective operation of both functions are considered.

TABLE III. SPECIFICATIONS OF HARDWARE SETUP

Specifications of Loads			
	Phase A	**Phase B**	**Phase C**
Critical Load	(68 + *j* 116) // 80 Ω (resistive plus inductive)	(68 + *j* 116) // 100 Ω (resistive plus inductive)	(68 + *j* 116) // 120 Ω (resistive plus inductive)
Noncritical Load	40 Ω (resistive)	40 Ω (resistive)	40 Ω (resistive)
Specifications of the Grid			
Power Source	Vg = 220 V (RMS)		
Distribution Line	0.8 Ω, 10 mH		
Specifications of the 3-ph ES			
LC Filter	L = 0.5 mH, C = 13.2 uF		
Switching frequency	30 kHz		
Battery Storage	120 V × 2		

1) Voltage Support and Current Balancing

The power supply is programmed to emulate an ac mains with a mains voltage at the PCC slightly lower than the nominal value ($|V_n|$ = 220 V). The tests are conducted with (i) uncompensated state for the first t = 0 s to 60 s on the left hand side, (ii) the voltage support function only for the second t = 0 s to 60 s on the right hand side, (iii) current balancing function only for 60 s < t < 120 s, and (vi) simultaneous current balancing and voltage support functions for t > 120 s. The measurements of the ac mains voltage (Fig. 12), neutral current (Fig. 13), source currents (Fig. 14), and ES voltage (Fig. 15) have been captured.

For first t = 0 to 60 s, the system operates in the uncompensated state as the 3-ph ES stays in idle. The asymmetrical critical load results in the neutral current of 2.18 A (RMS), as given in Fig. 13. Due to the different loading in each phase, the mains voltages (Fig. 12) are lower than the nominal value for different amounts. The negative- and zero-sequence components of source current are not zero in Fig. 14. For second t = 0 to 60 s, 3-ph ES is activated to support the mains voltages. The ES voltages in Fig. 15 are unequal among three phases due to the different voltage deviations of mains voltage. Results in Fig. 12 shows that the 3-ph mains voltages are supported to the nominal value of 220 V. The voltage support function in three phases is helpful in reducing the neutral current. As indicated in Fig. 13, the neutral current drops to 0.88 A (59.6% reduction). For t = 60 to 120 s, the voltage support function of the 3-ph ES is turned off, and the power balancing function is turned on. The ES voltage is re-adjusted to perform the current balancing function, as shown in Fig. 15. The mains voltages (Fig. 12) are slightly lower than the nominal value but are much balanced. The neutral current (Fig. 113) drops to 0.02 A (RMS), almost a 100% reduction. In Fig. 14, the negative- and zero-sequence components of source currents are reduced to near zero. In the final stage (t = 120 to 180 s), both functions of current balancing and voltage support are activated. The 3-ph ES voltage is adjusted again into a new state, as shown in Fig. 15. The 3-ph mains voltages (Fig. 12) are compensated to the nominal value. The neutral current (Fig. 13) is satisfactorily reduced to 0.07 A (RMS). The negative- and zero-sequence components of source currents in Fig. 14 are compensated to near zero.

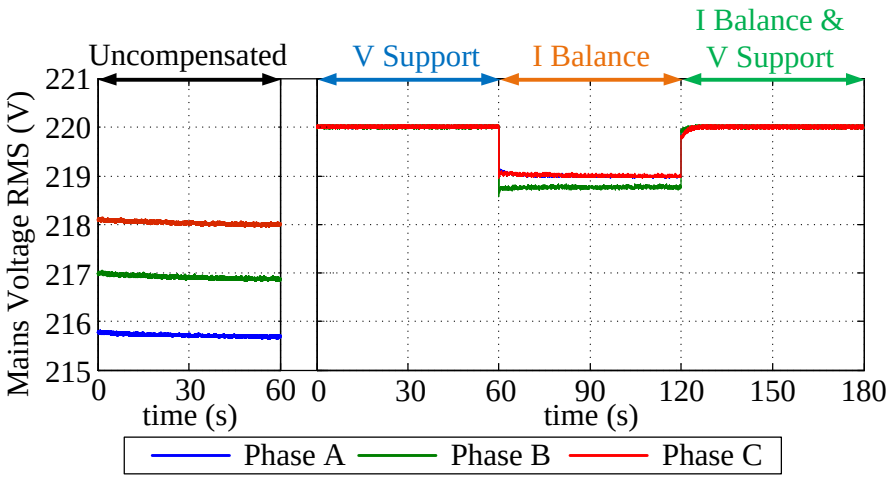

Fig. 12. Measured 3-ph mains voltages.

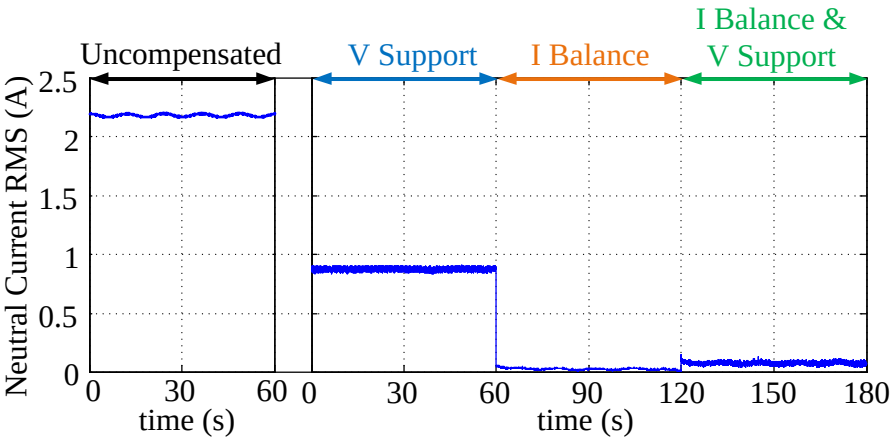

Fig. 13. Measured neutral current.

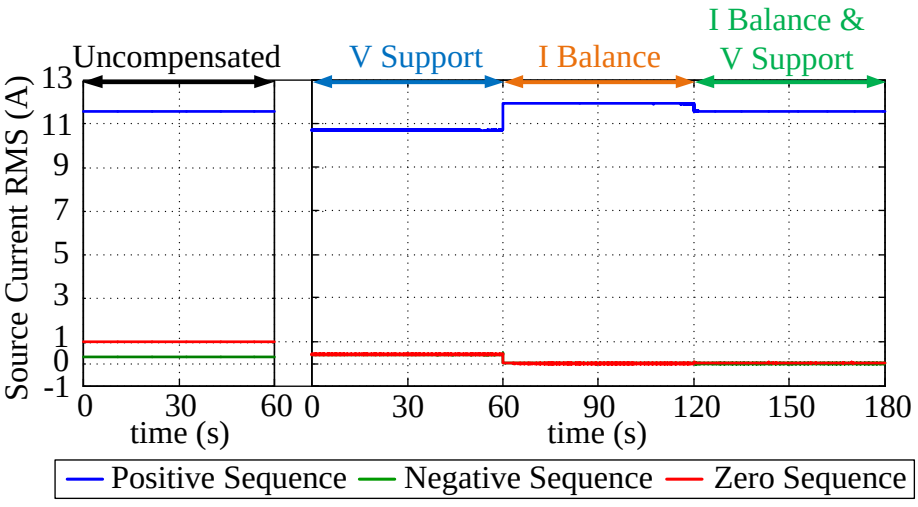

Fig. 14. Measured source currents (positive-, negative-, and zero-sequence components).

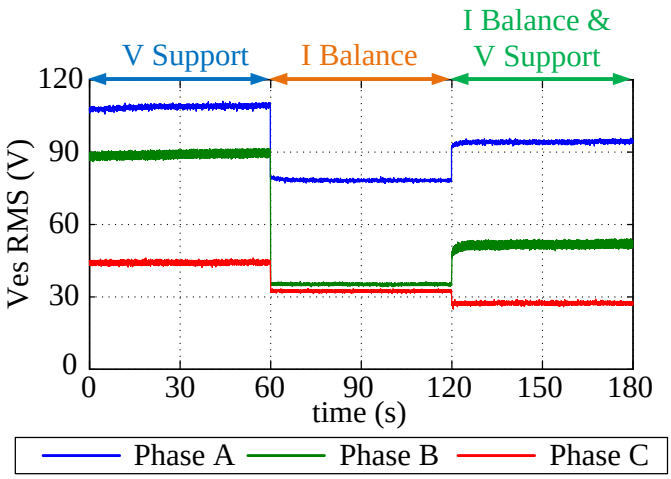

Fig. 15. Measured 3-ph ES voltages.

2) Voltage Suppression and Current Balancing

The second set of tests are conducted with (i) uncompensated state for the first t = 0 s to 60 s on the left hand side, (ii) the voltage suppression function only for the second t = 0 s to 60 s on the right hand side, (iii) current balancing function only for 60 s < t < 120 s, and (vi) simultaneous current balancing and voltage suppression functions for t > 120 s. The power source is programmed to set the ac mains voltage slightly higher than its nominal values ($|V_n|$ = 220 V). The measurements of the ac mains voltage (Fig. 16), neutral current (Fig. 17), the source currents (Fig. 18), and ES voltage (Fig. 19) are included.

In the first 0 < t < 60 s, the uncompensated mains voltages (Fig. 16) are higher than the nominal value for different amounts. The neutral current (Fig. 17) is 2.15 A (RMS). The source currents contain negative- and zero- sequence components as shown in Fig. 18. For the second t = 0 s to 60 s, the voltage suppression function of 3-ph ES is activated. An asymmetrical 3-ph ES voltage is inserted into the grid to suppress the ES voltages (Fig. 19). Therefore, the mains voltages (Fig. 16) are compensated to the nominal value. The neutral current (Fig. 17) drops for a noticeable amount to 0.81 A (62.3% reduction). For the t = 60 s to 120 s, the voltage suppression function of the 3-ph ES is deactivated, and the power

balancing function is turned on. The 3-ph ES voltage is modulated to a new asymmetrical state to fully compensate the negative- and zero-sequence current (Fig. 19). The mains voltages (Fig. 16) are slightly higher than the nominal value. The neutral current (Fig. 17) is satisfactorily reduced to 0.1 A (RMS). The negative- and zero-sequence components of source current is compensated to near zero as shown in Fig. 18. In the final stage (t = 120 s to 180 s), both voltage suppression and power balancing functions are turned on. The 3-ph ES voltage is adapted to perform dual functions (Fig. 19). The mains voltages (Fig. 16) are tightly regulated at the nominal value. The neutral current (Fig. 17) is well suppressed to 0.14 A (RMS). In Fig. 18, the negative- and zero-sequence components of source current are compensated to near zero.

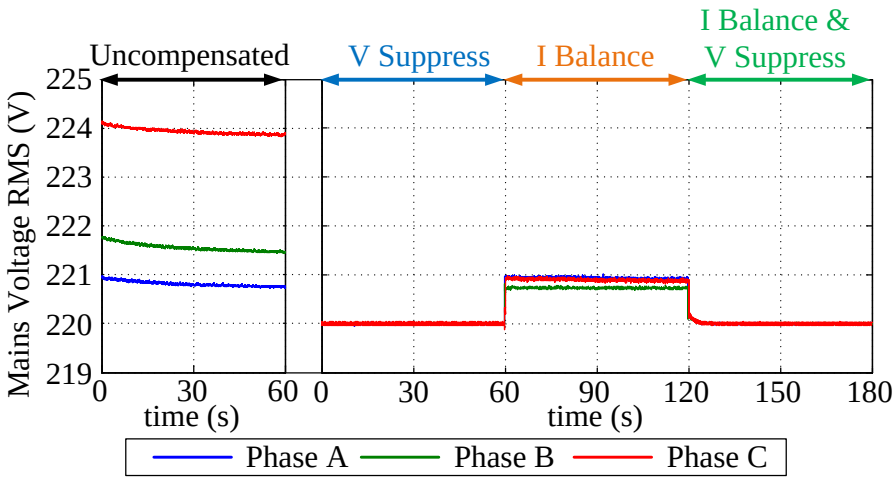

Fig. 16. Measured 3-ph mains voltages.

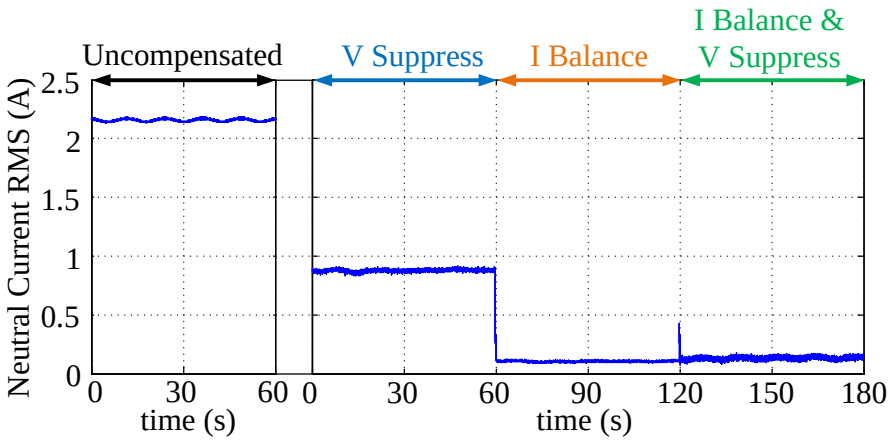

Fig. 17. Measured neutral current.

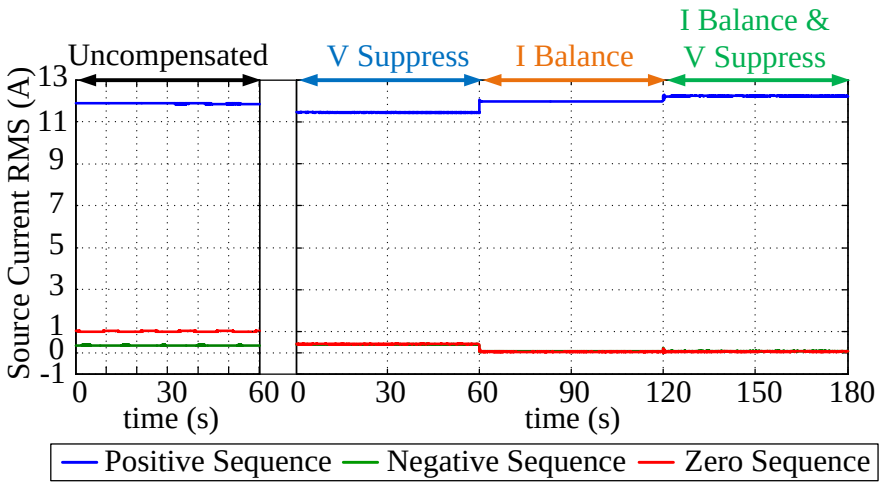

Fig. 18. Measured source currents (positive-, negative-, and zero-sequence components).

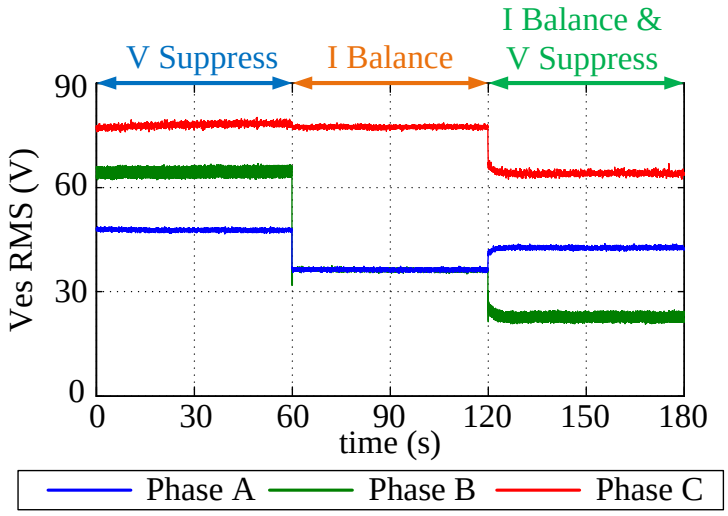

Fig. 19. Measured 3-ph ES voltage.

B. Tests on Instantaneous Power Optimization

In this section, the optimization approach discussed in Section III is implemented to reduce the average and oscillating power, whilst 3-ph ES is programmed to perform source current balancing. The hardware circuit is similar to the one in Fig. 11. The specifications are tabulated in TABLE IV. The 3-ph ES is the same as the one used in the last section. The control is implemented in the dSpace 1006.

Based on the circuit parameters given in TABLE IV, the active power of the 3-ph ES can be written as

$$\overline{P_{es}} = \left(x - 1.366\right)^2 + y^2 - 1.661 \tag{33}$$

Since the c=1.661 in (33) is larger than zero, it is possible to find an optimized ES voltage reference to achieve both zero average active power and minimal oscillating active power.

TABLE IV. SPECIFICATIONS OF THE SYSTEM SETUPS

Specifications of Loads			
	Phase A	**Phase B**	**Phase C**
Critical Load	115 Ω (resistive)	173.5 Ω (resistive)	77.2 Ω (resistive)
Noncritical Load	59.5 Ω (resistive)	59.5 Ω (resistive)	59.5 Ω (resistive)
Source Voltages	110 V ∠0°	120 V ∠240°	115 V ∠120°

In addition to the un-compensated state, the hardware system is tested for another three states by using the "Un-optimized", "Near-optimized", and "Optimized" ES voltage references as discussed in Section III. The experimental results of ES active power and source currents are recorded and compared in Fig. 20 and Fig. 21, respectively.

In Fig. 20, the source current in positive-, negative, and zero-sequences are recorded for four different circuit states. The un-compensated system has a 0.32 A negative- and zero-sequence currents as indicated by respectively the green and red trace in Fig. 20(a). All three sets of ES voltage references ("Un-optimized" in Fig. 20(b), "Near-optimized" in Fig. 20(c), and "Optimized" in Fig. 20(d)) are able to remove the negative- and zero-sequence components from the source currents. Hence, in the aspect of source current balancing, the three sets of ES voltage references show no apparent difference.

The key difference of three sets of ES voltage references reflects on their ability in handling the instantaneous active power. In Fig. 21, the waveforms of the instantaneous active power of 3-ph ES with different sets of voltage references are recorded. It can be found that the active power of 3-ph ES with "Near-optimized" and "Optimized" ES voltage references has a near zero average active power, as indicated by the green and red trace respectively. However, the active power of the 3-ph ES with "Un-

optimized" references have a much larger average active power, as indicated by the blue trace. The amplitude of the oscillation is also more dramatic in the active power of the 3-ph ES with "Un-optimized" reference than the other two. Comparing the green and the red trace in Fig. 21, one can find the amplitude of the active power oscillation of the 3-ph ES with "Optimized" references is smaller than the one with "Near-optimized" references. Thus, it is confirmed that the power optimization approach can effectively reduce the average active power and dampen the oscillating power when 3-ph ES is performing source current balancing.

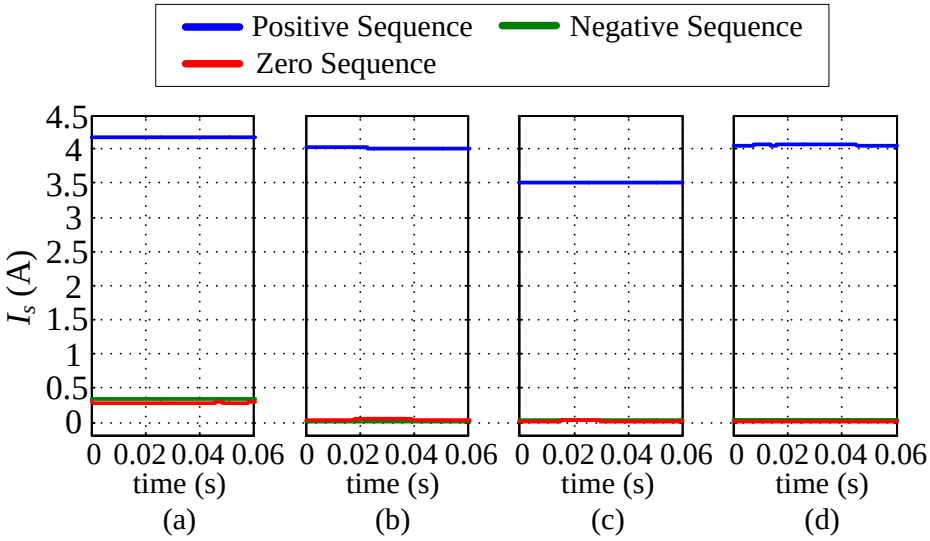

Fig. 20. Positive-, negative-, and zero-sequence source currents. (a) Un-compensated. (b) Un-optimized. (c) Near-optimized. (d) Optimized.

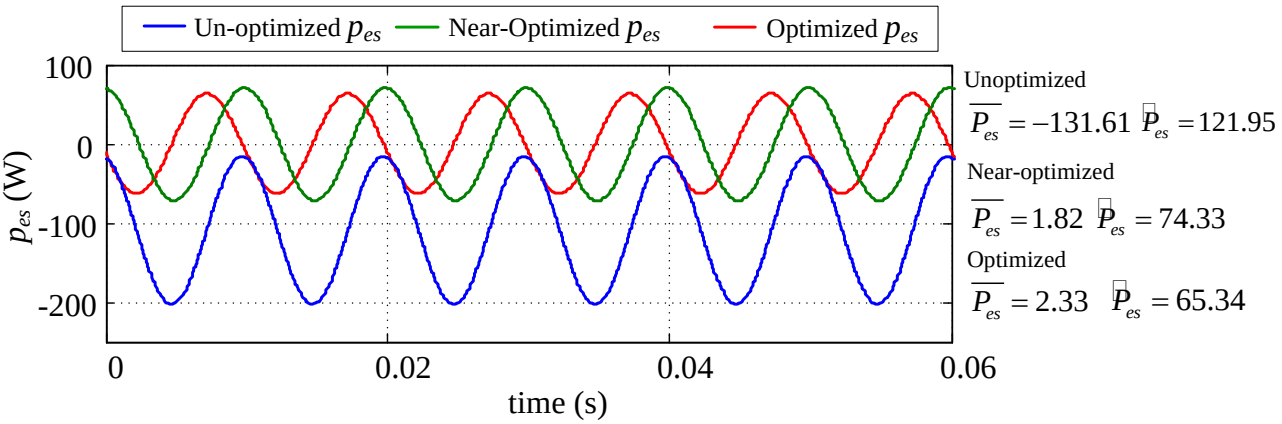

Fig. 21. The instantaneous active power of 3-ph ES. (Note: $\overline{P_{es}}$ and $\tilde{P}_{es}$ are respectively the DC offset and the amplitude of sinusoidal waveforms.)

VI. CONCLUSIONS

Using the Instantaneous Power Theory as the theoretical framework, this paper analyzes the use of 3-ph ES in providing multiple functions of voltage regulation and reduction of power imbalance and oscillating active power. The conditions for minimizing the average and oscillating power have been derived for the first time. Not only does the analysis provides the analytic solution to maintain the power balance in a 3-ph system as previously reported in [18], it also allows one to minimize the oscillating active power. The analysis enables the integration of multifunctional controls in a single controller. The analysis and the proposed control scheme have been practically verified in a hardware setup. The practical measurements show that multiple objectives can be achieved simultaneously.

ACKNOWLEDGEMENT

The authors are grateful to the Hong Kong Research Grant Council for its support of the Theme-based Research Project (T23-701/14-N).

REFERENCES

[1] C. Hochgraf and R. H. Lasseter, "Statcom controls for operation with unbalanced voltages," *IEEE Transactions on Power Delivery,* vol. 13, pp. 538-544, 1998.

[2] H. Akagi, "Active Harmonic Filters," *Proceedings of the IEEE,* vol. 93, pp. 2128-2141, 2005.

[3] I. Axente, J. N. Ganesh, M. Basu, M. F. Conlon, and K. Gaughan, "A 12-kVA DSP-Controlled Laboratory Prototype UPQC Capable of Mitigating Unbalance in Source Voltage and Load Current," *IEEE Transactions on Power Electronics,* vol. 25, pp. 1471-1479, 2010.

[4] Hirofumi Akagi, Edson H. Watanabe and Mauricio Aredes, "The Instantaneous Power Theory," in *Instantaneous Power Theory and Applications to Power Conditioning*, ed: Wiley-IEEE Press, 2007, pp. 41-107.

[5] X. Guo, W. Liu, and Z. Lu, "Flexible Power Regulation and Current-limited Control of Grid-connected Inverter under Unbalanced Grid Voltage Faults," *IEEE Transactions on Industrial Electronics* (early access).

[6] J. Miret, A. Camacho, M. Castilla, L. G. d. Vicuña, and J. Matas, "Control Scheme With Voltage Support Capability for Distributed Generation Inverters Under Voltage Sags," *IEEE Transactions on Power Electronics,* vol. 28, pp. 5252-5262, 2013.

[7] P. Rodriguez, A. V. Timbus, R. Teodorescu, M. Liserre, and F. Blaabjerg, "Flexible Active Power Control of Distributed Power Generation Systems During Grid Faults," *IEEE Transactions on Industrial Electronics,* vol. 54, pp. 2583-2592, 2007.

[8] K. Ma, W. Chen, M. Liserre, and F. Blaabjerg, "Power Controllability of a Three-Phase Converter With an Unbalanced AC Source," *IEEE Transactions on Power Electronics,* vol. 30, pp. 1591-1604, 2015.

[9] F. Nejabatkhah, Y. W. Li, and B. Wu, "Control Strategies of Three-Phase Distributed Generation Inverters for Grid Unbalanced Voltage Compensation," *IEEE Transactions on Power Electronics,* vol. 31, pp. 5228-5241, 2016.

[10] X. Guo, W. Liu, X. Zhang, X. Sun, Z. Lu, “Flexible control strategy for grid-connected inverter under unbalanced grid faults without PLL,”IEEE Trans. Power Electron., vol. 30, no. 4, pp. 1773–1778, Apr. 2015.

[11] C. A. Hill, M. C. Such, D. Chen, J. Gonzalez, and W. M. Grady, "Battery Energy Storage for Enabling Integration of Distributed Solar Power Generation," *IEEE Transactions on Smart Grid,* vol. 3, pp. 850-857, 2012.

[12] P. P. Varaiya, F. F. Wu, and J. W. Bialek, "Smart Operation of Smart Grid: Risk-Limiting Dispatch," *Proceedings of the IEEE,* vol. 99, pp. 40-57, 2011.

[13] S. Y. Hui, C. K. Lee, and F. F. Wu, "Electric Springs—A New Smart Grid Technology," *IEEE Transactions on Smart Grid,* vol. 3, pp. 1552-1561, 2012.

[14] Q. Wang, M. Cheng, and Z. Chen, "Steady-State Analysis of Electric Springs With a Novel δ Control," *IEEE Transactions on Power Electronics,* vol. 30, pp. 7159-7169, 2015.

[15] D. Chakravorty, B. Chaudhuri, and S. Y. R. Hui, "Rapid Frequency Response From Smart Loads in Great Britain Power System," *IEEE Transactions on Smart Grid* (early access).

[16] Q. Wang, M. Cheng, and Y. Jiang, "Harmonics Suppression for Critical Loads Using Electric Springs With Current-Source Inverters," *IEEE Journal of Emerging and Selected Topics in Power Electronics,* vol. 4, pp. 1362-1369, 2016.

[17] S. Yan, S. C. Tan, C. K. Lee, B. Chaudhuri, and S. Y. R. Hui, "Electric Springs for Reducing Power Imbalance in Three-Phase Power Systems," *IEEE Transactions on Power Electronics,* vol. 30, pp. 3601-3609, 2015.

[18] K. T. Mok, S. S. Ho, S. C. Tan, and S. Y. Hui, "A Comprehensive Analysis and Control Strategy for Nullifying Negative- and Zero-Sequence Currents in an Unbalanced Three-Phase Power System Using Electric Springs," *IEEE Transactions on Power Electronics* (early access).

[19] Y. Zheng, D. J. Hill, K. Meng, and S. Y. R. Hui, "Critical Bus Voltage Support in Distribution Systems with Electric Springs and Responsibility Sharing," *IEEE Transactions on Power Systems* (early access).

[20] C. K. Lee, B. Chaudhuri, and S. Y. Hui, “Hardware and control implementation of electric springs for stabilizing future smart grid with intermittent renewable energy sources,” *IEEE Transactions on Power Electronics,* vol. 1, no. 1, pp. 18–27, Mar. 2013.

[21] S. Yan, S. C. Tan, C. K. Lee, B. Chaudhuri, and S. Y. Ron Hui, "Use of smart loads for power quality improvement," *IEEE Journal of Emerging and Selected Topics in Power Electronics,* vol. 5, no. 1, pp. 504-512, Dec. 2016.

[22] X. Yuan, J. Allmeling, W. Merk, and H. Stemmler, “Stationary-frame generalized integrators for current control of active power filters with zero steady state error for current harmonics of concern under unbalanced and distorted operation conditions,” *IEEE Transactions on Industrial Application*, vol. 38, no. 2, pp. 523–532, Mar./Apr. 2002.

[23] X. Guo, W. Liu, X. Zhang, X. Sun, and Z. Lu, “Flexible control strategy for grid-connected inverter under unbalanced grid faults without PLL,” *IEEE Transactions on Power Electronics*, vol. 30, no. 4, pp. 1773–1778, Apr. 2015.